Mobility functions for [001] CSL grain boundaries in Ni from molecular dynamics

Etienne Ngenzi, Zakaria El Omari, Brigitte Bacroix, Sylvain Queyreau

Mobility functions for [001] CSL grain boundaries in Ni from molecular dynamics

Etienne Ngenzi*[1], Zakaria El Omari[2], Brigitte Bacroix[2], and Sylvain Queyreau[1]

[1] *Université Sorbonne Paris Nord, LSPM, CNRS UPR 3407*
[2] *LSPM, CNRS UPR 3407, Université Sorbonne Paris Nord*

December 31, 2021

Abstract

Molecular Dynamics (MD) studies of grain boundary migration in polycrystalline materials provide fundamental insights into the origin of complex dependence of grain boundary mobility on both motive force and temperature. In this study, we systematically investigated the motion of [001]CSL grain boundaries in pure nickel over a range of temperature $[100-1000]$K and motive force $[50-500]$MPa. We explored a large part of the fundamental zone of $\Sigma5$, $\Sigma13$ and $\Sigma25$, thus covering both symmetric tilt, twist and mixed characters. This study shows that the dependence of grain boundary mobility on temperature can deviate from Arrhenius-type dependence. It also reveals that upon increasing driving force, the dependence of grain boundary velocity on motive force changes from exponential to linear. As we explored stress-temperature parametric space in detail, identification of kinetic regimes has permitted to propose phenomenological laws of velocity function of temperature and motive force. Since atomistic modelling yield detailed information about the migration process down to the atomistic length scale, developed velocity functions can serve as input in large scale simulations of microstructure evolution.

1 Introduction

Microstructure evolution of a polycrystalline materials during processing can have a significant influence on their mechanical response. Since, microstructure of polycrystals is made of a network of Grain Boundaries (GB) i.e interfaces between differently oriented grains, grain boundary motion plays a major role in microstructure evolution. Thus, understanding and predicting grain boundary motion are central tasks in metal processing [1–6]. Over the past decade, both quantitative and qualitative description and prediction of GB motion under various thermo-mechanical loading conditions have been studied from computational [7–11] and experimental [3, 12–15] point of views. Qualitative predictions of grain boundary evolution is often made based on very simple form for the mobility function (M). However, a more quantitative description would require a detailed understanding of the dependence of GB motion on various factors. Indeed, both experimental and computational investigations on bi-crystalline and polycrystalline materials attempt at connecting the evolution of mobility functions to five geometrical macroscopic degrees of freedom of a grain boundary [3, 16], to impurity content [17], to boundary shape [18, 19], to temperature[20, 21] and to driving forces [9, 22]. Although, mobility is easily defined from a simple empirical relation (equation 1) between grain boundary velocity v and driving force P [23], for some GBs, mobility manifests complex dependence on temperature and often deviates from the expected Arrhenius type equation [20].

$$v = MP \tag{1}$$

For example, some grain boundaries exhibit a mobility, which is insensitive to temperature change (called hereafter athermal) and some other grain boundaries are associated to a mobility corresponding to thermal damping (antithermal)[24, 25]. Until now, the reason behind these different temperature dependence of the mobility of GB with temperature remains mostly not understood. Both recent experimental [23, 26] and computational [20, 25, 27] studies have attempted to link the mobility evolution to the atomic structure of GB. For example, some studies have related athermal motion to low energy faceted grain boundaries which move via the propagation of either steps or secondary grain boundary dislocations [23, 27–30]. The temperature dependence of the velocity may not be unique for a given GB (as described by its macroscopique DOF). For example, atomic simulations [24, 25] have shown that $\Sigma5(210)$ exhibits a thermally activated motion at lower temperature while it responds differently at higher temperatures and this effect was related to a change in the GB atomic structure. This emphasises once more the importance of the GB atomistic structure on their (macroscopic) properties and behaviour.

Another key parameter in the mobility function may be the nature and amplitude of the motive force as it was recognised long ago [31]. The motion of

*Corresponding author: etienne.ngenzi@univ-paris13.fr

some GBs is coupled with a tangential translation of one grain with respect to its adjacent grain[7]. Since then, both theoretical, experimental and computational studies [7, 22, 32–35] conducted on this so-called shear coupled grain boundary motion, and this type of migration is certainly one of the most studied type of grain boundary motion. MD simulations have revealed that GB with this type of motion moves in either stick-slip or stop-go fashion [7, 36] with a tangential velocity of the form:

$$v_t = \beta v \tag{2}$$

in which β is a geometric factor[37]. On the other hand, the lack of linear dependence of velocity on driving force can also originate from the magnitude of the applied motive force. Studies of Deng et al.[9], Lacasta et al.[38] and Constantini et al.[39] have evidenced that dependence. Those studies revealed a linear relationship when applied stress is either sufficiently smaller ($P < k_BT$) so that atoms only oscillate around their equilibrium positions with occasional jump of the energy barrier back and forth in a random manner or larger enough ($P > k_BT$) so that a large number of atoms have enough mechanical energy to escape energy barrier. At intermediate stress, velocity deviates from a linear correlation.

In recent years, some systematic studies have been conducted on vast panel of GB configurations (few hundreds) in order to determine major trends in both static and dynamic properties [25]. Such studies demonstrate once again the complexity of describing grain boundary properties and the importance of taking into account the atomic configuration of grain boundary in describing these properties [40]. Investigations that covered a wide range of the Fundamental Zone (FZ), which represents the symmetries of the underlying CSL structure of a grain boundary have applied a specific magnitude of driving force for different temperatures. Although some major trends can be seen by simplifying the results a bit, the evolution of mobility of some GB remain still unclear, in particular as function of the temperature.

In this work, we performed Molecular Dynamics(MD) systematic study of the motion of [001]Σ GBs in pure nickel spanning a very broad range of temperatures and motive forces. The GB configurations investigated encompass various CSL GBs with low Σ values with both low and high misorientation angles. We investigated both pure tilt and twist characters along with mixed characters, thus covering a large part of the FZ of the corresponding Σ GB. The initial configurations are carefully chosen. we explored the temperature-stress parametric space in a systematic manner. For that, a detailed map of this space will allow to find major trends that are common for several grain boundaries rather than some particular behaviours for a specific grain boundary. It also allows identification of dynamic transition of kinetic regimes that may occur under various circumstances. Based on these trends and dynamic transitions, we will rationalise our results and propose phenomenological laws for the GB velocity as function of motive force and temperature that can be used in larger-scale simulations. The paper is organised as follows: after this introductory section, we give a detailed methodology in section 2 showing how simulations are conducted. In section 3.1, we provide details of how velocity is extracted from raw MD data and provide mobility signatures of representative grain boundaries followed by proposition of phenomenological laws of migration in section 3.2, after we provide the elementary mechanisms of migration of representative grain boundaries in section 3.3. We finalise with a discussion in section **??** and the conclusions in section 4.

2 Methodology

In order to perform a systematic study of the GB migration in well controlled conditions, we reprise the bicrystalline geometry employed in a number of simulation studies [4, 22, 25, 41, 42]. A planar GB is introduced in the centre of the simulation box with a normal direction along the y-axis of the simulation cell. The use of Periodic Boundary Conditions (PBC) along x and z axes allows for representing a semi-infinite domain. Free Surfaces (FS) is employed on y simulation faces, and for that, we made sure that the y cell dimensions are large enough to prevent the interaction between GB and FS when the GB is in motion. Our simulation box setup is illustrated in figure 1. Great

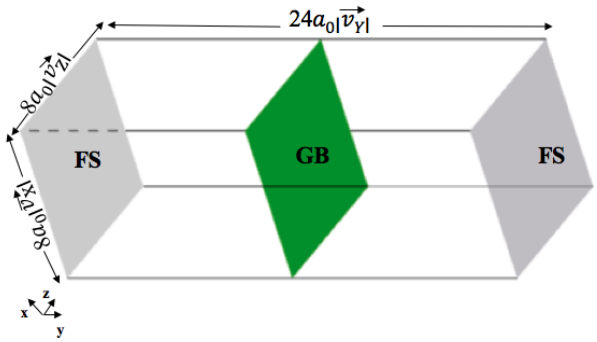

Figure 1: The simulation setup used in this work. $\vec{v}_X, \vec{v}_Y$ and $\vec{v}_Z$ stand for the CSL vectors along the X, Y and Z directions respectively and a_o is the lattice parameter. Free surface are shown in a grey colour and the grain boundary is shown in green colour.

care has been taken to construct the atomistic structure of GBs. For this, we used our own tool to build CSL GB with arbitrary (rational) orientation. This tool relies upon determining the natural CSL vectors of the considered Σ structure to properly orient both grains with respect to the simulation box. These vectors are also used to properly place the PBC faces in order to preserve the continuity of atomic structure across PBC. This can also be seen as a practical way to solve the underlying and coupled sets of diophantine equations associated to PBC on both rotated grains.

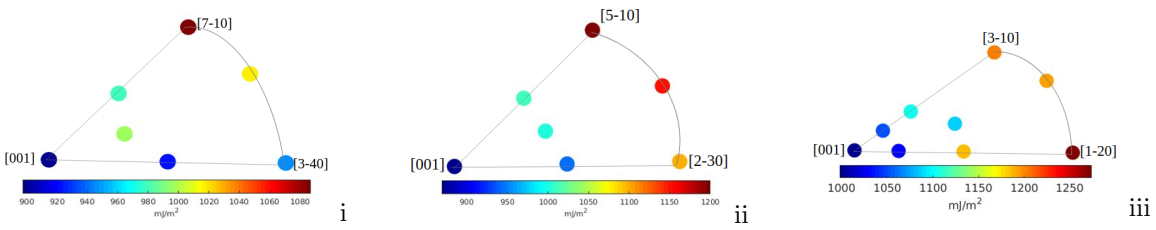

Figure 2: List of all investigated grain boundaries of i) Σ25, ii) Σ13 and iii) Σ5, shown using the fundamental zone representation of their grain boundary normal along with their energy in a colour code, from dark blue (low energy) to dark red (high energy).

This tool is similar to the seminal work of Patala et a.[43], with the difference that the procedure steps are done in a slightly different order to be able to preserve rectangular geometry of the simulation box. This tool will be the subject of a forthcoming publication. Figure 2 shows grain boundaries that we have built in fundamental zone representation of their grain boundary normal. We have carefully selected atomic potential. Interatomic interactions between Ni atoms were described using a multibody semi-empirical potential from Foiles [44], which is based on EAM formalism [45]. This Ni potential was parametrized in part to recover Rose's state equation [46] and was specifically derived for mechanical application. In particular, it allows to reproduce elastic constants and stacking fault energy values of Ni. This potential is thus well adapted for mechanical studies and have been employed in several studies of grain boundary migration.

Finding the atomic structure corresponding to the ground state of a GB from the initial construction described above remains a challenging task. This is due to additional microscopic degrees of freedom of grain boundaries. Thus, several atomic configurations are possible for a given macroscopic configuration [47, 48]. To address this, Frolov and Mishin [49] and Banadaki et al.[50] performed semi-grand and grand canonical Monte Carlo (MC) simulations, respectively; and show that one grain boundary can have several atomic structures that may differ from the known structures of the studied GBs. In this work, to sample a number of different initial configurations, here we have employed a more practical solution, commonly used in literature [25, 42, 48] as a trade off between accuracy and numerical cost. We shift one lattice with respect to an other along the CSL basis vectors within the GB plan. During translation steps, neighbouring grains may contain atoms that are physically too close. The overlapping atoms are resolved by removing one of the atoms from the system. To this end, we have constructed at least 100000 initial grain boundary structures for each grain boundary. To determine the boundary energy, we performed conjugate-gradient minimisation for all sets of initial grain boundary structures at 0K. Figure 3 shows the GB excess energy mapping, represented with a colour code of i)$\Sigma5(1\bar{2}2)$ mixed,ii) $\Sigma5(1\bar{2}0)$ symmetric tilt and iii) $\Sigma5(001)$ pure twist grain boundary as example. Since the dynamics of a grain boundary strongly depends on its atomic configuration, we have carefully selected grain boundary configurations to use in MD simulations. From the 2D energy map, the configuration with the lowest energy were selected as the right candidate for MD. Figure 2 shows energy of the selected stable configurations of i) Σ25, ii) Σ13 and iii) Σ5. To validate our selection, we compared our GB energy measures from values reported in literature when available. Our results were in a good agreement with values reported by Olmsted et al.[42].

Great care has also been taken for MD simulation conditions. In our MD calculations, we have used an NVT ensemble since there is no clear dependence of grain boundary mobility on thermodynamic ensemble [10]. The selected stable configurations at 0K were heated and expanded to the desired temperature and respective lattice parameter over a period of 125ps. After, the selected configurations were equillibrated to the desired temperature for 125ps before applying a motive force. To keep the correct dynamical atomic structure during simulation (see references [5, 24] for more details), we performed a convergence test to determine the size of our simulation cell in each direction within the GB plane. The total cell size was at least 8 repeat units of the grain boundary periodic structure (as detailed in [51]). To move a grain boundary, we employed the synthetic driving force method developed by Janssens et al. [10] implemented within LAMMPS [52]. This methods has been tested, validated and used in many studies [4, 10, 20, 27, 42]. The results from synthetic driving forces have been reported to be in a good agreement with results obtained with other motive forces [8, 10, 21]. In the present study, simulations were allowed to run for 200ps, or until the boundary reaches the end of a simulation box. For each grain boundary, we considered 3 or 4 different temperatures from 100K up to 1000K while remaining below the melting point of Nickel which is 1726K[53]. In all simulations, we applied synthetic motive forces that should correspond to stresses in a range of 50 to 500 MPa. In total, we performed 1250 simulations of GB motion.

3 Results

The results from our static calculations emphasise the importance of carefully choosing initial configuration

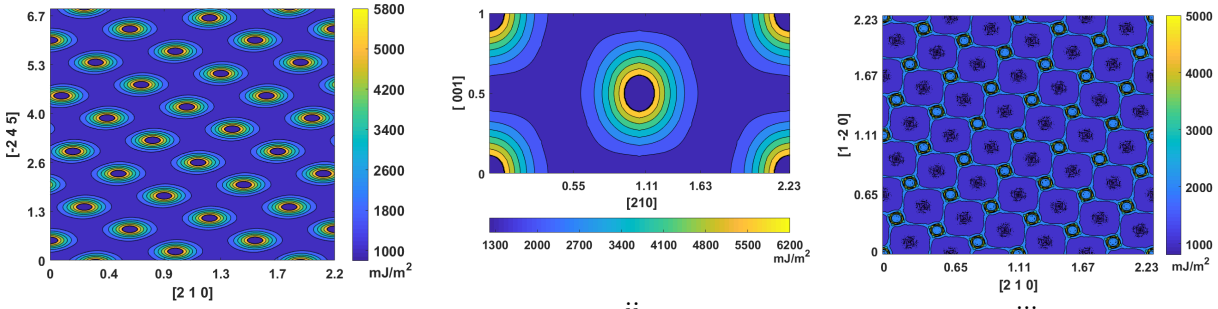

i ii iii

Figure 3: Energy distribution on the surface of Σ5 i) mixed $(1\bar{2}2)$ ii) $(1\bar{2}0)$ symmetric tilt and iii) (001) pure twist GBs represented with a colour code, from blue (low energies) to yellow (high energies), as the top grain is translated relative to the bottom grain by CSL vectors along the grain boundary plane.

of a grain boundary. GB energy strongly depends on its microscopic degrees of freedom. The trend in energy distribution on the surface of a grain boundary varies as well from one GB to another (compare Σ5 in figure 3iii from Σ13 pure twist in figure 12 in the appendix B[4]) and from one grain boundary character to another (tilt, mixed or twist) as figures 3i to 3iii show. This distribution is always symmetric recovering the symmetric nature of underlying CSL lattice. Overall, the energy of the most stable configuration strongly depends on orientation of a grain boundary plane. For all grain boundaries studied a general trend emerges. The GB energy smoothly increases or decreases monotonically across the fundamental zone (figures 2i to 2iii). Pure twist and tilt grain boundaries are typically the minimum and maximum energy respectively.
To investigate dynamic properties, MD simulations were run long enough and regardless of the applied stress and temperature, configuration data were extracted every one picosecond. To locate a grain boundary in our simulation box, we have first used a common neighbour analysis (CNA) algorithm [54] implemented in Open Visualisation Tool (OVITO)[55] to identify all atoms belonging to the grain boundary. The position (x_i) of each atom i was then recorded every time t_j. The average position of a grain boundary (X_{t_j}) is calculated as $X_{t_j} = \frac{1}{n}\sum_{i=1}^{n} x_i$ which is barycenter of atomic positions of n atoms belonging to grain boundary at time t_j.

3.1 Velocity of a grain boundary

From grain boundary positions, velocity is extracted as the derivative of the displacement-time curve. Thus, the velocity is slope of displacement-time curve at each temperature and applied stress. Figure 4 shows displacement-time curves of Σ5$(1\bar{2}2)$ mixed grain boundary illustrating the dependence of that slope on temperature and motive force. All processed outputs, regardless of the magnitude of applied stress, were qualitatively classified into 4 categories based on temperature dependence. The first category contains all grain boundaries which exhibit a thermally activated motion i.e. velocity increases with increasing temperature for the same applied stress (figure 5a).

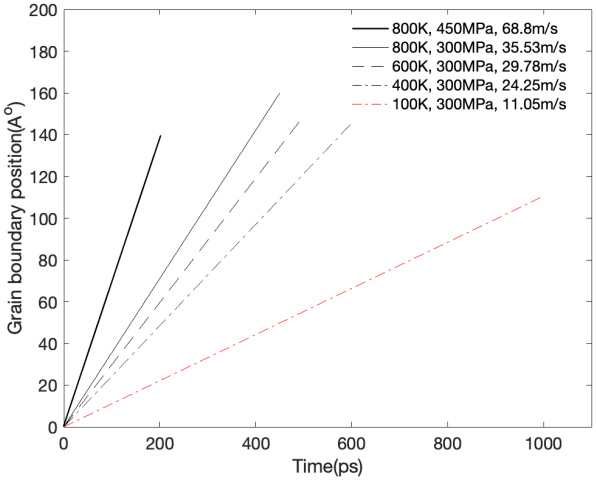

Figure 4: GB displacement versus time of Σ5$(1\bar{2}2)$at 800K. The grain boundary velocity is slope of the curve.

The second contains only Σ5$(3\bar{1}3)$ mixed grain boundary. It has velocity which is insensitive to temperature change. The grain boundary that behaved in this fashion was denoted athermal (figure 5b) in literature [25]. The inset to the figures 5a and 5b shows the same data points in a zoomed in semi-logarithmic scale in attempt to facilitate the visualisation. The third group comprises grain boundaries with velocities decreasing with increasing temperature i.e. antithermal grain boundary. All pure tilt grain boundaries belonging to Σ25 counting 13% of all GBs, behaved in this fashion. Figure 5c shows velocity curves of Σ25$(3\bar{4}0)$ symmetric tilt grain boundary representative of other antithermal grain boundaries. The last group denoted as others, contains one exceptional grain boundary Σ5$(1\bar{2}0)$. It behaved in a fashion that could not be classified in any general trend stated above for the whole range of temperature and stress. It is thermally activated at lower temperature and antithermal at higher temperature.

Regarding the velocity dependence on applied motive force, 82.6% GBs have an exponential relationship between applied driving force and velocity for the entire

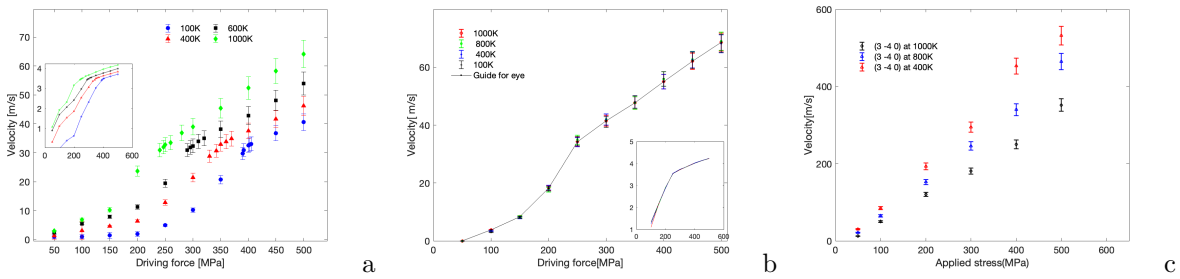

Figure 5: Velocity versus driving forces of a) pure twist $\Sigma5(001)$ b) mixed $\Sigma5(3\bar{1}3)$ and c) symmetric tilt $\Sigma25(3\bar{4}0)$ grain boundaries at different temperatures. The inset to figure a and b shows the same data on a semi-logarithmic scale for a better identification of the transition.The error bars show an estimate of one standard deviation in the measured velocity.

range of motive force and 8.7% have both exponential and linear regimes. The rest has only linear regime. From figures 5a and 5b, both regimes can be visually identified for both $\Sigma5(001)$ and $\Sigma5(3\bar{1}3)$. Initially, an exponential regime at lower stresses and then a linear regime at higher stresses. To facilitate identification of this dynamic transition, the same data in figure 5a and 5b are presented in the inset to figure 5a and 5b respectively in a semi-logarithmic scale. The transition stresses and velocities mark the starting point at which the velocity function changes from concave to linear due to a change in local derivative of velocity function of motive force. Transition stresses and velocity depend on grain boundary structure and temperature. For instance, for pure twist $\Sigma5$ and $\Sigma13$, transition stress is linearly related to temperature whereas it remains constant for athermal $\Sigma5(3\bar{1}3)$ as figure 6 shows. The variation of transition stress function of temperature follows a generalised equation 3, where α_γ and α_{γ_o} are constants and their values are given in appendix A[4] for each grain boundary studied.

$$P^*(T) = -\alpha_\gamma T + \alpha_{\gamma_o} \tag{3}$$

From now on, we will refer to the applied motive force as P, transition stress as P^*, and simulation temperature as T.

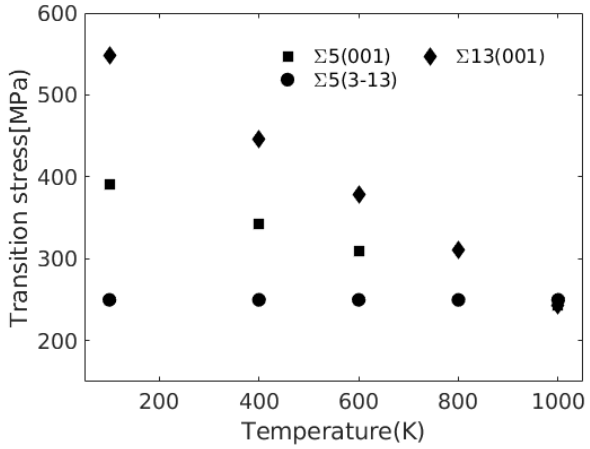

Figure 6: Transition stress versus temperature for $\Sigma5$, $\Sigma13$ pure twist and mixed $\Sigma5(3\bar{1}3)$ grain boundaries.

3.2 Proposing phenomenological law for predicting velocity

Identification of kinetic regimes in velocity curve permitted developing laws for predicting velocity in the stress and temperature range investigated. These functions do not only allow us to rationalise the origin of these dynamic transitions but also can serve as input in larger scale models of microstructure evolution since they require detailed inputs from MD simulations. In this section, we show our procedure step by step. We start with GBs whose velocity-stress curves exhibit both regimes and lastly GBs whose velocity is linearly related to applied stress for the entire range investigated. Based on experimental studies [23], mobility in the exponential regime can be described by Arrhenius relation (equation 4).

$$M(P,T) = \frac{A}{P^*} exp(-\frac{\Delta G(P,T)}{k_B T}) \tag{4}$$

Where $\Delta G(P,T)$ is the Gibbs free energy (equation 5), k_B is the Boltzmann constant and A is a constant.

$$\Delta G(P,T) = \Delta H - T\Delta S \tag{5}$$

ΔH and ΔS are enthalpy and entropy of activation for grain boundary migration respectively. Next, we combined equations 1, 4 and 5 to give Arrhenius relation of GB velocity in the exponential regime. Based on an assumption that for the case of dislocation, the motion is controlled by a single migration mechanism, the enthalpy of activation in equation 5 was predicted using empirical relation of Kocks, Argon, and Ashby [56], shown in equation 6. It is worthy noting that ΔH expression takes into account the contribution of mechanical work provided to the system through applied driving force.

$$\Delta H = \Delta H_o[1 - (\frac{P}{P^*})^p]^q \tag{6}$$

Where ΔH_o is the activation enthalpy at zero effective stress and p, q are fitting parameters such that $0 < p \leq 1$ and $1 \leq q \leq 2$ [56]. With regard to experimental study of Spitzig on dislocations [57], we have further assumed the entropy change (ΔS) to be negligible compared to the activation energy (enthalpy) for migration (ΔH). Consequently, ΔS was discarded

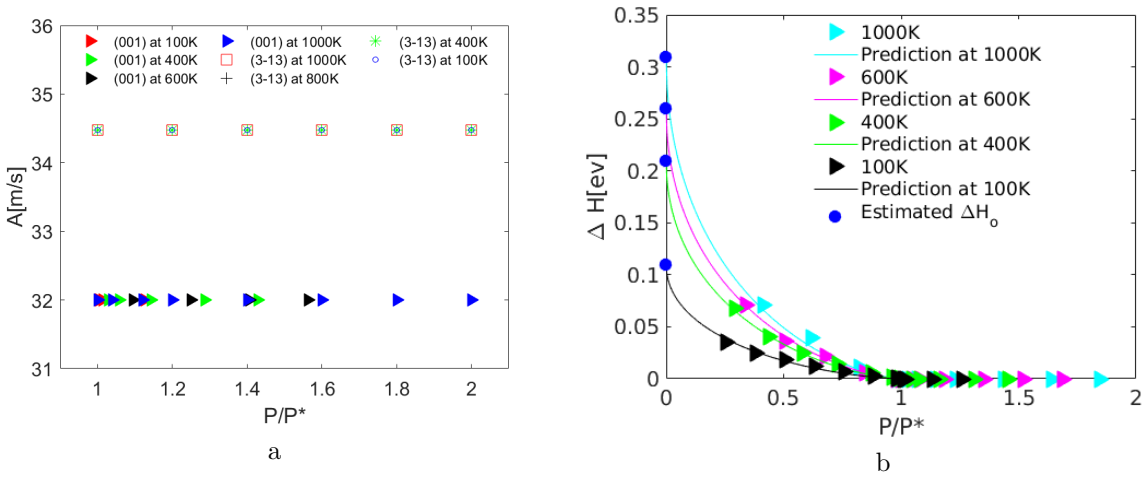

Figure 7: a) Plot of the value of constant A versus the normalised stress for $\Sigma5(001)$ pure twist and $\Sigma5(3\bar{1}3)$ mixed grain boundary at different temperatures b) Comparison between MD and predicted enthalpy of activation of $\Sigma5$ pure twist at different temperatures.

from equation 5. We performed a global least squares fit to the raw data to determine p and q. For ΔH_o, we used the value of ΔH at zero effective stress for each temperature. For all GBs investigated, ΔH_o takes a wide range of values between 0.0006 and $1.5eV$. To adduce athermal GB to exhibit lower ΔH_o value compared from other grain boundaries. The relationship between ΔH_o and temperature was observed to be linear and follow equation 7.

$$\Delta H_o(T) = \alpha_H T + \alpha_{H_o} \tag{7}$$

Where α_H and α_{H_o} are constants and their values are given in appendix A for each grain boundary investigated. Interestingly, we obtained almost similar values of p and q for all GBs which are ≈ 0.5 and ≈ 1.5 respectively. To validate this model, we compared estimated values with raw data from MD. Figure 7 shows how parameters in our model are identified from raw data of MD. We first verified that A from MD raw data is constant for all temperatures. Figure 7a, indeed, confirms that A is temperature insensitive. As expected, the A of athermally activated motion is higher than that of thermally activated migration mechanism. Next, we compared the estimated values of ΔH from calculated ΔH from raw data of MD. Figure 7b shows estimation of three parameters(p,q and ΔH_o) in equation 6 for $\Sigma5$ pure twist representative of other thermally activated grain boundaries. It is evident that estimated ΔH is in good agreement with ΔH from MD velocity data.

At motive force P $\geq P^*$, due to dynamic transition, the relationship between velocity and driving force is linear. This linear regime could be fitted using equation 8.

$$v(P,T) = A(\frac{P}{P^*})^k \tag{8}$$

Where k is a constant which does not depends on temperature nor on magnitude of driving force. To make sure of this linearity, we have fitted equation 8 to linear data set. We, indeed, obtained $k \approx 1$. Hence, the final velocity function in the linear regime is given by equation (9).

$$v(P,T) = \frac{AP}{P^*} \tag{9}$$

By combining the final equations from both exponential and linear regimes, a general closed-form velocity function of stress and temperature is

$$v(P,T) = \begin{cases} \frac{AP}{P^*} exp(-\frac{\Delta H_o}{k_B T}(1-(\frac{P}{P^*})^p)^q), & \text{if } P < P^* \\ \frac{AP}{P^*}, & \text{if } P \geq P^* \end{cases}$$

Where parameters (A, P^*, ΔH_o) in equation depend on grain boundary and two parameters p and q are fitting parameters. Finally, to validate our procedure, we have compared predicted velocity from MD raw data. Figures 8a and 8b show comparison between MD and predicted velocity of thermally activated $\Sigma5(001)$ pure twist and athermal $\Sigma5(3\bar{1}3)$ mixed grain boundaries. It is clear that the predicted and MD velocities are in good agreement. For antithermal GBs, we have exploited the proportionality between velocity and motive force. We have fitted a linear equation 10 to MD velocity. β is a constant that linearly depends on temperature.

$$v(P,T) = \frac{P}{\beta} \tag{10}$$

Where $\beta = c_\beta T + \beta_o$ in which c_β and β_o are constants whose values are given in Appendix A^4. Figure 8c shows agreement between MD and predicted velocity for $\Sigma25(3\bar{4}0)$ representative of other antithermal grain boundaries at different temperatures and motive forces.

3.3 Migration mechanism

If trends in migrations are clearly categorised, one can be able to find a clear correlation with elementary mechanism origins which explain these categories.

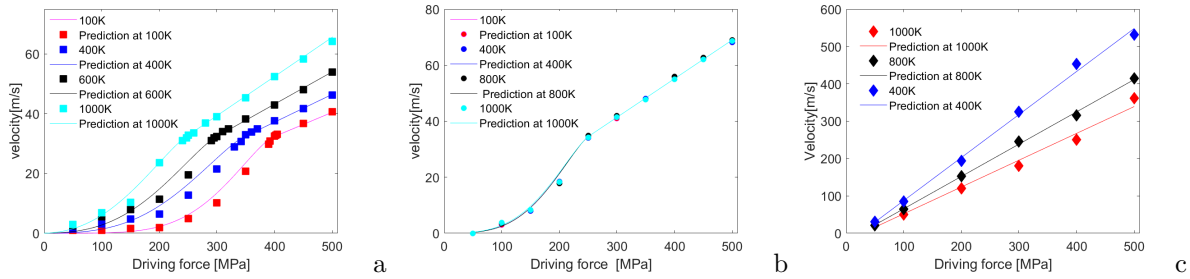

Figure 8: Comparison between MD and predicted velocity for a) thermal $\Sigma5(001)$ pure twist b) athermal $\Sigma5(3\bar{1}3)$ mixed and c) antithermal $\Sigma25(3\bar{4}0)$ grain boundaries.

For that, we investigated grain boundary migration mechanisms. By analysing atomic structure of grain boundary as it migrates, GB displacement is mediated by the deformation and rotation/translation of the grain boundary structural units. The grain boundary moves by jumping from one most energetically stable structural unit to another. The duration of such jumps depends on the magnitude of driving force and temperature. For all tilt GBs which count 39% of all investigated GBs, the change in grain boundary surface and the normal GB displacement are accommodated by a relative in-plane translation of the shrinking crystal. Although this type of migration is beyond the scope of this paper, it is important to show illustration of this type of migration as it shows the impact of motive force on grain boundary migration. In the appendix C^4, figures 13 a to f shows shear coupled migration of $\Sigma5(1\bar{2}0)$ STGB at 100K and 400MPa which is representative of all other shear coupled grain boundaries. For the majority of GBs, the motion was

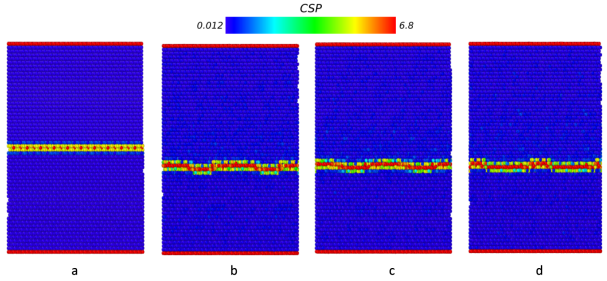

Figure 9: Migration of pure twist $\Sigma5$ mediated by nucleation and propagation of disconnection. Atoms are colored by centro-symmetric Parameter (CSP) where blue atoms are in perfect FCC positions and the rest belongs to the defect. Note that two periodic images of the simulation cell are shown for the sake of a better visualisation. Figures show a) simulation cell before nucleation of disconnection b) after nucleation of disconnections c) and d) growth of a disconnection.

rarely planar over a large area. Rather, a critical area of the GBs goes first (figure 9b) that propagate (figures 9c to d) . This disconnection is due to local atomic shuffling that causes a relatively small in-plane atomic displacements accommodated by transformation/translation of a grain boundary structural unit. When all structural units in the GB undergo this transformation/translation i.e when the growth of a nucleated disconnection spans the simulation box, a grain boundary copes with by making a complete step forward. In all investigated grain boundaries, 82.6% (mostly $\Sigma5$ and $\Sigma13$) which are thermally activated move by nucleation and propagation of disconnections. We have also observed that the magnitude of applied driving force influences the number of nucleation sites of disconnections. This number increases with the ratio $\frac{P}{P^*}$. If $\frac{P}{P^*} \geq 1$, the grain boundary moves as a whole as transformation/translation occurs simultaneously in all structural units and if $\frac{P}{P^*} \leq 1$, the grain boundary is rarely flat due to nucleation of disconnections on random sites. This subject is beyond the scope of this paper, more details on this will be subject of the forthcoming publications.

On the other hand, we have observed two groups of grain boundaries in which the transformation of GB structural units occurs simultaneously. The first groups contains all antithermal grain boundaries. The transformation is due to an array of grain boundary dislocations that simultaneously glide. Hence, the grain boundary surface remains flat during migration. Figure 10 shows dislocation gliding in $\Sigma25(7\bar{1}0)$ STGB which is representative of other antithermally activated grain boundaries. The second group contains only one

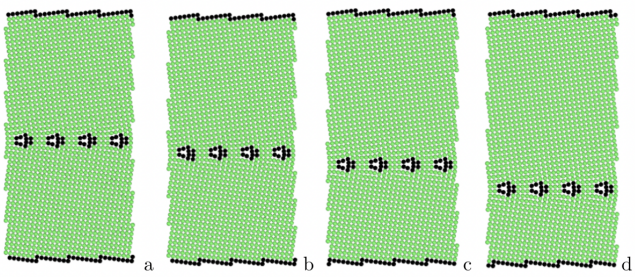

Figure 10: Dislocation gliding in $\Sigma25(7\bar{1}0)$ at 100K for 200MPa. Atoms are in green and black colours for FCC position and defect respectively.

GB which already has several disconnections at its surface. This GB moves almost as a whole due to activation and propagation of multiple disconnections. The same grain boundary is shown in figures 11a to 11d which show propagation of disconnections. Atoms are coloured by the centro-symmetric parameter(CSP) with dark blue corresponding to perfect FCC positions and the rest for the defect. Figure 11a which corre-

sponds to initial GB configuration shows that disconnections are already in the GB surface before propagation, and the applied driving force propagates them across the entire periodic box (figure 11b and 11c) to reach a next stable configuration (figure 11d) by making a complete step forward.

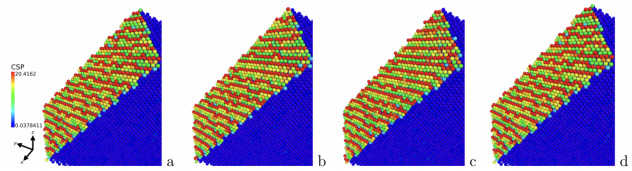

Figure 11: Propagation of $\Sigma5(3\bar{1}3)$ mixed GB at 200MPa for 400K. Atoms are coloured by the centro-symmetry parameter(CSP),atoms in positions FCC are shown in blue a) shows the grain boundary before migration b) and c) during propagation of disconnections d) across the entire periodic box.

4 Conclusion

In summary, we have systematically explored the driving force - temperature parametric space. We have investigated at least one GB of each character in the fundamental zone of $\Sigma5$, $\Sigma13$ and $\Sigma25$. This study provides more details of the mobility dependence on both temperature and driving force. The main findings can be summarised in three main points: 1) Although velocity is often linearly related to applied stress, there are in fact two regimes depending on stresses and temperature. At lower applied stresses, velocity appears to be an exponential function of the applied stress whereas at higher stress, it is a monotonic linear function of applied stresses. In addition, the exponential regime is broad at lower temperature and becomes narrower with increasing temperatures. 2) Based on curves of enthalpy of activation, two kinetic regimes correspond to two different migration mechanisms. Before transition stress, the migration of a GB necessitates a critical activation energy whereas past transition stress, any provided mechanical work is sufficient enough to overcome energy barrier. 3)Phenomenological functional mobility laws are provided for both regimes. They are derived from fitting physically based expressions to the data points from molecular dynamics simulations. In this study, we have only studied grain boundaries of different character with misorientation angle in range $[16.3° - 73.7°]$ around [001]. However, the sample is still too limited to demonstrate the generality of major trends observed here. This indicates the need for further studies of GB with different misorientation axis to verify the general trends observed here.

Appendix A

We give values of all parameters appearing in equations of dependence of transition stress P^* and enthalpy of activation at zero effective stress ΔH_o on temperature along with the values of other constants in the proposed phenomenological law for all investigated grain boundaries. The empty spaces mean that the corresponding parameter does not appear in the equation or a different equation was proposed. The empty spaces appears only for $\Sigma25$ as this type contains many antithermal grains boundaries. On the other hand, the majority of grain boundaries of type $\Sigma5$ and $\Sigma13$ are thermally activated and exhibit both exponential and linear regime in the considered stress range or beyond that range. Symmetric tilt grain boundaries have a wide exponential regime compared from mixed and pure twist characters.

$\Sigma5$					
Plane	$\frac{\alpha_H}{10^{-4}}$	$\frac{\alpha_{Ho}}{10^{-3}}$	α_γ	$\frac{\alpha_{\gamma_o}}{10^3}$	$\frac{A}{10^2}$
(001)	2.0	117.4	0.17	0.4	0.32
$(1\bar{2}0)$	4.2	20.0	0.42	4.30	42.40
$(1\bar{2}1)$	2.5	43.5	2.70	6.52	29.20
$(1\bar{2}2)$	3.2	17.9	1.30	5.82	22.00
$(3\bar{1}0)$	3.0	27.3	1.17	5.04	44.30
$(3\bar{1}8)$	2.7	29.3	0.54	4.42	20.70
$(3\bar{1}3)$	6.0	0.00	0.00	0.25	0.34
$(4\bar{3}0)$	3.5	15.0	2.50	3.41	36.80
$(4\bar{3}3)$	2.1	8.00	1.50	2.40	23.40

$\Sigma13$					
Plane	$\frac{\alpha_H}{10^{-4}}$	$\frac{\alpha_{Ho}}{10^{-2}}$	α_γ	$\frac{\alpha_{\gamma_o}}{10^3}$	$\frac{A}{10^2}$
(001)	2.0	13.3	0.34	0.58	2.80
$(2\bar{3}0)$	2.0	34.3	0.7	4.70	42.60
$(2\bar{3}3)$	2.0	33.5	1.2	7.50	21.20
$(5\bar{1}0)$	3.0	27.2	1.8	5.23	41.90
$(5\bar{1}3)$	3.0	15.4	0.3	3.44	33.20
$(7\bar{4}0)$	2.9	15.1	2.5	8.50	70.00
$(7\bar{4}6)$	3.0	18.4	4.5	9.30	33.20

$\Sigma25$							
Plane	$\frac{\alpha_H}{10^{-4}}$	$\frac{\alpha_{Ho}}{10^{-3}}$	α_γ	$\frac{\alpha_{\gamma_o}}{10^3}$	$\frac{A}{10^3}$	$\frac{c_\beta}{10^{-3}}$	β_o
$(3\bar{4}0)$						9	0.52
$(3\bar{4}1)$	1	39.6	0.5	4.40	2.1		
$(7\bar{1}1)$	3	29.6	0.8	7	2.5		
$(2\bar{1}0)$						7	0.45
$(7\bar{1}0)$						2.6	1.54
$(10\bar{5}2)$	2	39.8	0.5	4.4	2.1		
(001)	2.7	18.3	0.63	0.88	0.7		

Appendix B

Microscopic degrees of freedom potentially influence grain boundary energy. Translating one grain boundary relative to its adjacent grain in a way that keeps misorientation between both grain create many configuration of similar macroscopic degrees of freedom. The energy of resulting grain boundary configurations is mapped on the surface of grain boundary to illustrate the role of microscopic degree of freedom in influencing the energetic of a grain boundary. As the underlying CSL lattice is symmetric , the resulting energy distribution is symmetric for all symmetric grain boundaries. However, the distribution depends on grain boundary type and character.

Appendix C

The migration of symmetric tilt grain boundaries in response to applied driving force is accompanied by a lateral displacement of the growing grain.

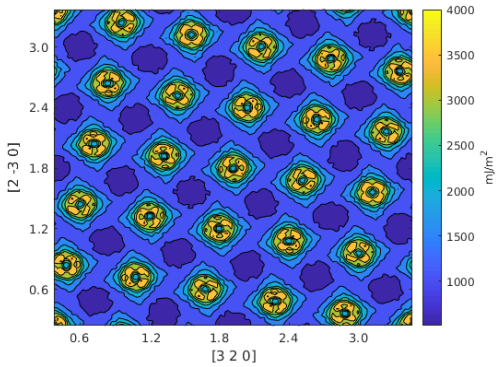

Figure 12: Energy map of Σ13 pure twist GB represented with a colour code, from blue (low energies) to yellow (high energies), as one grain is translated relative to the other by CSL vectors within the GB plane

.

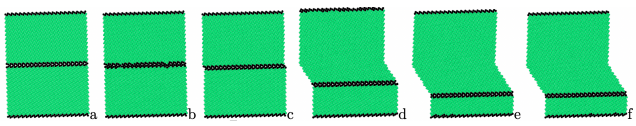

Figure 13: The mechanical response of $\Sigma5(1\bar{2}0)$ symmetric tilt grain boundary to applied driving force of 400MPa at 100K. The atoms in fcc position are green and the defect in black. a) before applying driving force b) during migration, showing rearrangement of the atomic configuration in the plane of the GB to form a new structural unit accommodated by a relatively smaller in plane translation of growing grain. c) when all structural units have undergone transformation and a grain boundary copes with by making one step forward d) to f) the shear-coupled migration of the GB in the bicrystal.

References

[1] S. Brandstetter, K. Zhang, A. Escuadro, J. Weertman, and H. Van Swygenhoven, Grain coarsening during compression of bulk nanocrystalline nickel and copper, *Scripta Materialia* **58**, 61 (2008).

[2] Z. Chen, F. Liu, H. Wang, W. Yang, G. Yang, and Y. Zhou, A thermokinetic description for grain growth in nanocrystalline materials, *Acta materialia* **57**, 1466 (2009).

[3] G. Gottstein and L. Shvindlerman, Thermodynamics, kinetics, applications (1999).

[4] D. L. Olmsted, E. A. Holm, and S. M. Foiles, Survey of computed grain boundary properties in face-centered cubic metals—ii: Grain boundary mobility, *Acta materialia* **57**, 3704 (2009).

[5] C. Race, J. von Pezold, and J. Neugebauer, Role of the mesoscale in migration kinetics of flat grain boundaries, *Physical Review B* **89**, 214110 (2014).

[6] A. P. Sutton, Interfaces in crystalline materials, *Monographs on the Physice and Chemistry of Materials* 349–352 (1995).

[7] J. W. Cahn, Y. Mishin, and A. Suzuki, Coupling grain boundary motion to shear deformation, *Acta materialia* **54**, 4953 (2006).

[8] C. Deng and C. A. Schuh, Atomistic simulation of slow grain boundary motion, *Physical Review Letters* **106**, 045503 (2011).

[9] C. Deng and C. A. Schuh, Diffusive-to-ballistic transition in grain boundary motion studied by atomistic simulations, *Physical Review B* **84**, 214102 (2011).

[10] K. G. Janssens, D. Olmsted, E. A. Holm, S. M. Foiles, S. J. Plimpton, and P. M. Derlet, Computing the mobility of grain boundaries, *Nature materials* **5**, 124 (2006).

[11] Z. T. Trautt, M. Upmanyu, and A. Karma, Interface mobility from interface random walk, *Science* **314**, 632 (2006).

[12] J. Brons and G. Thompson, A comparison of grain boundary evolution during grain growth in fcc metals, *Acta materialia* **61**, 3936 (2013).

[13] M. Legros, D. S. Gianola, and K. J. Hemker, In situ tem observations of fast grain-boundary motion in stressed nanocrystalline aluminum films, *Acta Materialia* **56**, 3380 (2008).

[14] T. Rupert, D. Gianola, Y. Gan, and K. Hemker, Experimental observations of stress-driven grain boundary migration, *Science* **326**, 1686 (2009).

[15] A. Rajabzadeh, F. Mompiou, S. Lartigue-Korinek, N. Combe, M. Legros, and D. Molodov, The role of disconnections in deformation-coupled grain boundary migration, *Acta Materialia* **77**, 223 (2014).

[16] G. Gottstein, D. Molodov, L. Shvindlerman, D. Srolovitz, and M. Winning, Grain boundary migration: misorientation dependence, *Current opinion in solid state and materials science* **5**, 9 (2001).

[17] D. Molodov, U. Czubayko, G. Gottstein, and

L. Shvindlerman, On the effect of purity and orientation on grain boundary motion, *Acta materialia* **46**, 553 (1998).

[18] M. Winning, G. Gottstein, and L. Shvindlerman, On the mechanisms of grain boundary migration, *Acta Materialia* **50**, 353 (2002).

[19] H. Zhang, M. Upmanyu, and D. Srolovitz, Curvature driven grain boundary migration in aluminum: molecular dynamics simulations, *Acta materialia* **53**, 79 (2005).

[20] E. R. Homer, E. A. Holm, S. M. Foiles, and D. L. Olmsted, Trends in grain boundary mobility: Survey of motion mechanisms, *Jom* **66**, 114 (2014).

[21] D. L. Olmsted, S. M. Foiles, and E. A. Holm, Grain boundary interface roughening transition and its effect on grain boundary mobility for nonfaceting boundaries, *Scripta Materialia* **57**, 1161 (2007).

[22] E. R. Homer, S. M. Foiles, E. A. Holm, and D. L. Olmsted, Phenomenology of shear-coupled grain boundary motion in symmetric tilt and general grain boundaries, *Acta Materialia* **61**, 1048 (2013).

[23] G. Gottstein and L. S. Shvindlerman, *Grain boundary migration in metals: thermodynamics, kinetics, applications* (CRC press, 2009).

[24] Y. Deng and C. Deng, Size and rate dependent grain boundary motion mediated by disconnection nucleation, *Acta Materialia* **131**, 400 (2017).

[25] E. R. Homer, S. Patala, and J. L. Priedeman, Grain boundary plane orientation fundamental zones and structure-property relationships, *Scientific reports* **5**, 15476 (2015).

[26] P. R. Cantwell, E. A. Holm, M. P. Harmer, and M. J. Hoffmann, Anti-thermal behavior of materials, *Scripta Materialia* **103**, 1 (2015).

[27] C. O'Brien and S. Foiles, Exploration of the mechanisms of temperature-dependent grain boundary mobility: search for the common origin of ultrafast grain boundary motion, *Journal of Materials Science* **51**, 6607 (2016).

[28] S. Babcock and R. Balluffi, Grain boundary kinetics—i. in situ observations of coupled grain boundary dislocation motion, crystal translation and boundary displacement, *Acta Metallurgica* **37**, 2357 (1989).

[29] J. Hirth, R. Pond, and J. Lothe, Disconnections in tilt walls, *Acta Materialia* **54**, 4237 (2006).

[30] S.-H. Jung, D. Y. Yoon, and S.-J. L. Kang, Mechanism of abnormal grain growth in ultrafine-grained nickel, *Acta materialia* **61**, 5685 (2013).

[31] D. W. Bainbridge, H. L. Choh, and E. H. Edwards, Recent observations on the motion of small angle dislocation boundaries, *Acta metallurgica* **2**, 322 (1954).

[32] D. Caillard, F. Mompiou, and M. Legros, Grain-boundary shear-migration coupling. ii. geometrical model for general boundaries, *Acta Materialia* **57**, 2390 (2009).

[33] D. Molodov, V. Ivanov, and G. Gottstein, Low angle tilt boundary migration coupled to shear deformation, *Acta Materialia* **55**, 1843 (2007).

[34] F. Mompiou, D. Caillard, and M. Legros, Grain boundary shear–migration coupling—i. in situ tem straining experiments in al polycrystals, *Acta Materialia* **57**, 2198 (2009).

[35] S. L. Thomas, K. Chen, J. Han, P. K. Purohit, and D. J. Srolovitz, Reconciling grain growth and shear-coupled grain boundary migration, *Nature communications* **8**, 1 (2017).

[36] A. Rajabzadeh, F. Mompiou, M. Legros, and N. Combe, Elementary mechanisms of shear-coupled grain boundary migration, *Physical review letters* **110**, 265507 (2013).

[37] J. W. Cahn and J. E. Taylor, A unified approach to motion of grain boundaries, relative tangential translation along grain boundaries, and grain rotation, *Acta Materialia* **52**, 4887 (2004).

[38] A. Lacasta, J. Sancho, A. Romero, and K. Lindenberg, Sorting on periodic surfaces, *Physical review letters* **94**, 160601 (2005).

[39] G. Costantini and F. Marchesoni, Threshold diffusion in a tilted washboard potential, *EPL (Europhysics Letters)* **48**, 491 (1999).

[40] L. Priester, *Grain boundaries: from theory to engineering*, vol. 172 (Springer Science & Business Media, 2012).

[41] R. Hadian, B. Grabowski, M. W. Finnis, and J. Neugebauer, Migration mechanisms of a faceted grain boundary, *Physical Review Materials* **2**, 043601 (2018).

[42] D. L. Olmsted, S. M. Foiles, and E. A. Holm, Survey of computed grain boundary properties in face-centered cubic metals: I. grain boundary energy, *Acta Materialia* **57**, 3694 (2009).

[43] A. D. Banadaki and S. Patala, An efficient algorithm for computing the primitive bases of a general lattice plane, *Journal of Applied Crystallography* **48**, 585 (2015).

[44] S. M. Foiles and J. Hoyt, Computation of grain boundary stiffness and mobility from boundary fluctuations, *Acta Materialia* **54**, 3351 (2006).

[45] M. S. Daw and M. I. Baskes, Embedded-atom method: Derivation and application to impurities, surfaces, and other defects in metals, *Physical Review B* **29**, 6443 (1984).

[46] J. H. Rose, J. R. Smith, F. Guinea, and J. Ferrante, Universal features of the equation of state of metals, *Physical Review B* **29**, 2963 (1984).

[47] A. Sutton, Rw balluffi interfaces in crystalline materials (1996).

[48] M. Tschopp and D. McDowell, Structures and energies of σ 3 asymmetric tilt grain boundaries in copper and aluminium, *Philosophical Magazine* **87**, 3147 (2007).

[49] T. Frolov, M. Asta, and Y. Mishin, Phase transformations at interfaces: observations from atomistic modeling, *Current Opinion in Solid State and*

Materials Science **20**, 308 (2016).

[50] A. D. Banadaki, M. A. Tschopp, and S. Patala, An efficient monte carlo algorithm for determining the minimum energy structures of metallic grain boundaries, *Computational Materials Science* **155**, 466 (2018).

[51] E. Homer, in *IOP Conf. Series: Mater. Sci. Eng* (2015), vol. 89, 012006.

[52] S. Plimpton, Fast parallel algorithms for short-range molecular dynamics, *Journal of computational physics* **117**, 1 (1995).

[53] D. Porter and K. Easterling, Phase transformations in metals and alloys (1992).

[54] A. Stukowski, Structure identification methods for atomistic simulations of crystalline materials, *Modelling and Simulation in Materials Science and Engineering* **20**, 045021 (2012).

[55] A. Stukowski, Visualization and analysis of atomistic simulation data with ovito–the open visualization tool, *Modelling and Simulation in Materials Science and Engineering* **18**, 015012 (2009).

[56] U. F. Kocks, A. AS, and A. MF, Thermodynamics and kinetics of slip (1975).

[57] W. Spitzig and A. Keh, Orientation dependence of the strain-rate sensitivity and thermally activated flow in iron single crystals, *Acta metallurgica* **18**, 1021 (1970).